Tsutomu HORI and Manami HORI
(Nagasaki Institute of Applied Science, Japan) April 2026, pp. 1 ~ 23

Simulations of Water Wave Generation caused by Running Hydrofoil by means of Wave-making Green's Function due to 2-D Vortex

by Tsutomu HORI † and Manami HORI ††

Summary

This paper conducts wave-making simulations for hydrofoils running at high speeds. The analysis is performed by constructing a wave-making Green's function due to a two-dimensional vortex filament by means of Fourier transform method. We adopt the developed Green's function as the kernel function, and approach the problem using the boundary element method. The Green's function is numerically computed by switching between three expansion forms, namely, Taylor expansion, continued fraction expansion, and asymptotic expansion, depending on the case.

Simulation calculations are performed on the lift and wave-making resistance acting on the hydrofoil, the generated wave profile, the flow velocity vectors and the pressure distribution around the hydrofoil. As a result, we gained concrete findings for the dependencies of wave-making phenomena upon the wing shape, forward speed, submerged depth, angle of attack and other factors.

Keywords : ***Simulations, Water Wave Generation, Running Hydrofoil, Wave-making Green's Function, 2-D Vortex***

1. Introduction

In recent years, hydrofoils have been increasingly attached on high-speed ships and oceanographic towed vehicles. Quantitatively understanding of the wave-making phenomena [(1), (2), (3)], which are generated when these hydrofoils run at high speeds near the water surface, is considered an important issue for evaluating their hydrodynamic performance.

In view of this situation, this paper conducts wave-making simulations for hydrofoils running at high speeds. The analysis is performed by constructing a wave-making Green's function due to a two-dimensional vortex filament by means of Fourier transform method. In the numerical calculation of

† *Professor Emeritus*, HORI's Laboratory of Ship Waves and Hydrostatic Stability, Nagasaki Institute of Applied Science, Japan

†† *Jewel Manami HORI of Five Stars JP,* Daughter of †

E-mail : milky-jun_0267.h@mxb.cncm.ne.jp
HomePage : https://www2.cncm.ne.jp/~milky-jun_0267.h/HORI-Lab/
(in Japanese)

Green's function, Taylor expansion is basically used, and in addition, continued fraction and asymptotic expansion are used in combination depending on the case. We adopt the developed Green's function as the kernel function, and approach the problem using the boundary element method.

Simulation calculations are performed on the lift and wave-making resistance acting on the hydrofoil, the generated wave profile, the flow velocity vectors and the pressure distribution around the hydrofoil. As a result, we gained concrete findings for the dependencies of wave-making phenomena upon the wing shape, forward speed, submerged depth, angle of attack and other factors.

Although these results are for two-dimensional wings, we believe some aspects may serve as foundational data for future hydrofoil research. We hereby report these findings and respectfully request the critique of experts in the field.

2. Wave-making Green's Functions due to 2-D Vortex Filament

Let us set up the boundary value problem for a two-dimensional running hydrofoil. As shown in Fig. 1, a hydrofoil of chord length c is placed in a uniform flow of velocity U with free surface and fluid density ρ at the submerged depth f and angle of attack α. Then, a Cartesian coordinate system places the origin o on the still water surface directly above the mid-chord of the hydrofoil, and sets the x-axis in the direction of uniform flow and the z-axis pointing vertically upward.

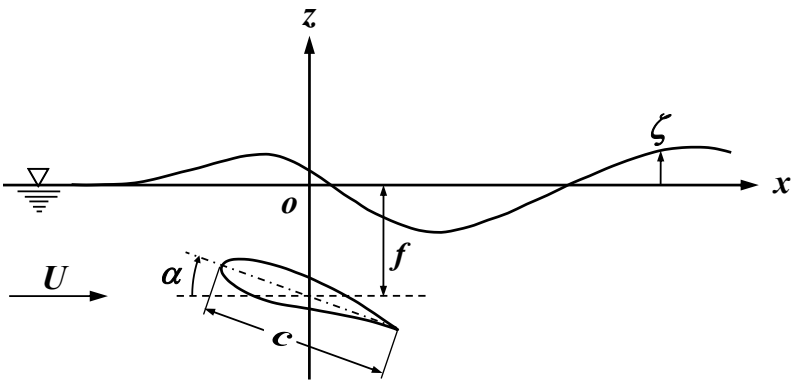

Fig. 1 Coordinate system and definitions of some basic quantities in the problem of hydrofoil.

2.1 Boundary value problem

The velocity potential Φ of the wavy flow field generated by a hydrofoil is composed by superposing the potential of the uniform flow and the disturbed potential ϕ, as follows :

$$\Phi(x, z) = Ux + \phi(x, z) \quad \cdots\cdots(1)$$

Below, we consider the conditions that this disturbed potential ϕ must satisfy. First, as the governing equation based on the continuity condition in the flow field, the Laplace's equation for ϕ must be satisfied in the entire region below the water surface, as follows :

$$[L] \quad \frac{\partial^2 \phi}{\partial x^2} + \frac{\partial^2 \phi}{\partial z^2} = 0 \quad (for \ z \le \zeta) \quad \cdots\cdots(2)$$

Here, ζ represents the displacement of the generated wave.

Next, assuming the linear free surface condition for the water surface $z=\zeta$, the following equation is imposed on the still water surface $z=0$.

$$\left.\begin{aligned} &[F]\quad \frac{\partial^2\phi}{\partial x^2}+\kappa_0\frac{\partial\phi}{\partial z}+\mu\frac{\partial\phi}{\partial x}=0 \quad (on\ z=0) \\ &\qquad where,\ \begin{cases} \kappa_0=\dfrac{g}{U^2}=\dfrac{1}{Fn^2c} \\ \mu\to+0 \end{cases} \end{aligned}\right\} \cdots\cdots(3)$$

In the above equation, κ_0 is the wave number, Fn is the Froude number defined by Eq. (61) later and g is the gravitational acceleration. And μ is Rayleigh's virtual friction coefficient, by which mathematically satisfies the radiation condition that no waves are generated upstream.

Furthermore, based on the assumption of infinite water depth, it is required that disturbance vanishes at the bottom of the water, as follows :

$$[B]\quad \left.\frac{\partial\phi}{\partial z}\right]_{z=-\infty}=0 \quad \cdots\cdots(4)$$

On the other hand, the boundary condition on the wing surface requires that the normal directional component of the flow is zero. Since it is written as $(U\boldsymbol{i}+\nabla\phi)\cdot\boldsymbol{n}=0$ if the outward-pointing unit normal vector on the wing surface is denoted by $\boldsymbol{n}=n_x\boldsymbol{i}+n_z\boldsymbol{k}$, the disturbed potential ϕ must satisfy the following equation :

$$[H]\quad \frac{\partial\phi}{\partial x}n_x+\frac{\partial\phi}{\partial z}n_z=-Un_x \quad \cdots\cdots(5)$$

In addition, at the trailing edge of the wing, the following conditions must be satisfied so that the flows on the face and back of the wing join smoothly :

$$[K]\quad Kutta\ Condition\ (at\ Trailing\ Edge) \quad \cdots\cdots(6)$$

In the analysis, the wave-making Green's function G due to a two-dimensional vortex filament, satisfying the above conditions [L], [F] and [B], is constructed in the next section. Then, the disturbed velocity potential ϕ is formed by placing n clockwise vortex filaments of strength Γ_j discretely on the wing surface $(\xi_j,-f_j)$, as follows :

$$\phi(x,z)=-\frac{1}{2\pi}\sum_{j=1}^{n}\Gamma_j G(x,z\,;\xi_j,-f_j) \quad \cdots\cdots(7)$$

At this time, the induced velocity in the direction of x and z can be computed respectively by using the following equation :

$$\left.\begin{aligned}\frac{\partial\phi}{\partial x} &= -\frac{1}{2\pi}\sum_{j=1}^{n}\Gamma_j\frac{\partial G(x,z;\xi_j,-f_j)}{\partial x}\\ \frac{\partial\phi}{\partial z} &= -\frac{1}{2\pi}\sum_{j=1}^{n}\Gamma_j\frac{\partial G(x,z;\xi_j,-f_j)}{\partial z}\end{aligned}\right\} \quad \cdots\cdots(8)$$

The boundary value problem is solved by numerically determining the vortex strength Γ_j using the method described in Chapter 3, such that the boundary condition [*H*] on the wing surface is satisfied.

2.2 Construction of wave-making Green's function

As shown in Fig. 2, the wave-making Green's function G of a counterclockwise two-dimensional vortex filament of strength $\Gamma=-2\pi$ placed at position $(\xi,-f)$ with submerged depth f is constructed in the following form [4] :

$$\begin{aligned}G(x,z) &= \theta + G'(x,z)\\ &= \tan^{-1}\frac{z+f}{x-\xi} + G'(x,z;\xi,-f)\end{aligned} \quad \cdots\cdots(9)$$

The principal solution θ can be formally expressed as a Fourier integral for the region $z+f>0$ including the water surface, as follows :

$$\theta = \tan^{-1}\frac{z+f}{x-\xi} = -\operatorname{Im}\left[\int_0^\infty e^{-k(z+f)+ik(x-\xi)}\cdot\frac{dk}{k}\right]_{z+f>0} \quad \cdots\cdots(10)$$

Here, Im[···] means taking the imaginary part inside the brackets.

Corresponding to the above equation, the regular part G' is also assumed in the following form, so as to satisfy the water's bottom condition [*B*] in Eq. (4).

$$G' = \operatorname{Im}\left[\int_0^\infty \psi(k)\, e^{kz+ikx}dk\right] \quad \cdots\cdots(11)$$

The undetermined kernel function $\psi(k)$ is easily solved so as to satisfy the free water surface condition [*F*] in Eq. (3), as follows :

$$\psi(k) = \frac{k+\kappa_0-i\mu}{k(k-\kappa_0-i\mu)}\cdot e^{-kf-ik\xi} = \left(-\frac{1}{k}+\frac{2}{k-\kappa_0-i\mu}\right)\cdot e^{-kf-ik\xi} \quad \cdots\cdots(12)$$

Here, the latter expression above is obtained by expanding the former into partial fractions, while μ in the numerator set to zero.

Substituting the above $\psi(k)$ back into G' in Eq. (11), it can be written as follows :

$$G' = -\operatorname{Im}\left[\int_0^\infty e^{-k(f-z)+ik(x-\xi)}\cdot\frac{dk}{k}\right]_{f-z>0} + 2\operatorname{Im}\left[\int_0^\infty \frac{1}{k-(\kappa_0+i\mu)}\, e^{-k(f-z)+ik(x-\xi)}dk\right] \quad \cdots\cdots(13)$$

Here, for the 1st term, since $f-z$ is positive under the water surface, it can be expressed using an arctangent function, similar to Eq. (10).

Now, let us consider the semi-infinite integral with respect to k in the above 2nd term by extending it onto the complex plane $k+im$ (5-a). When the integral path goes around the 1st quadrant for the downstream side $x-\xi>0$ and the 4th quadrant for the upstream side $x-\xi<0$, the integral at infinity disappears respectively. Accordingly, the integral with respect to k on the real axis can be transformed into an integral with respect to m on the imaginary axis. In this case, since the simple pole $\kappa_0+i\mu$ is located in the 1st quadrant, the residue only generates for downstream $x-\xi>0$. Therefore, setting the virtual friction coefficient $\mu\to+0$ and combining the positive and negative cases of $x-\xi$, this integral with k can be evaluated as follows (6-a) :

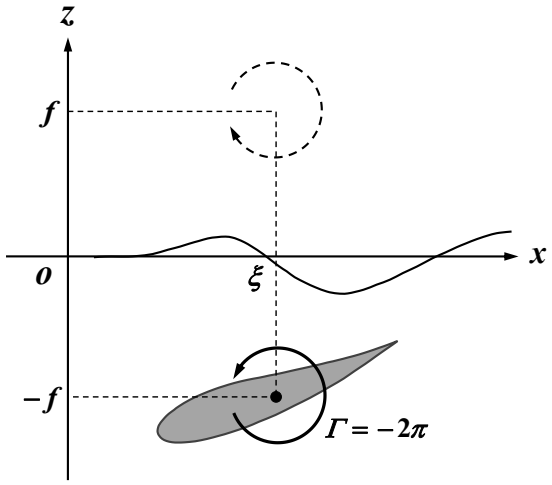

Fig. 2 Coordinate system of Green's function for an vortex filament.

$$\int_0^\infty \frac{e^{-k(f-z)+ik(x-\xi)}}{k-(\kappa_0+i\mu)}\,dk = \begin{cases} \displaystyle\int_0^\infty \frac{e^{-m|x-\xi|-im(f-z)}}{m+i\kappa_0}\,dm + 2\pi i\, e^{-\kappa_0(f-z)+i\kappa_0(x-\xi)} & (for\ x-\xi\ge 0) \\ \displaystyle\int_0^\infty \frac{e^{-m|x-\xi|+im(f-z)}}{m-i\kappa_0}\,dm = \overline{\int_0^\infty \frac{e^{-m|x-\xi|-im(f-z)}}{m+i\kappa_0}\,dm} & (for\ x-\xi<0) \end{cases}$$

$$= \mathrm{Re}\left[\int_0^\infty \frac{e^{-m|x-\xi|-im(f-z)}}{m+i\kappa_0}\,dm\right] + i\,\mathrm{sgn}(x-\xi)\cdot\mathrm{Im}\left[\int_0^\infty \frac{e^{-m|x-\xi|-im(f-z)}}{m+i\kappa_0}\,dm\right]$$

$$+\pi i\, e^{-\kappa_0(f-z)+i\kappa_0(x-\xi)}\cdot\left\{1+\mathrm{sgn}(x-\xi)\right\} \quad \cdots\cdots\cdots (14)$$

Here, $\overline{(...)}$ means taking the complex conjugate. And $\mathrm{sgn}(x-\xi)$ is signum function and takes +1 or -1 depending on the positive or negative values of $x-\xi$.

Therefore, since G' in Eq. (13) takes the imaginary part, the 1st term in Eq. (14) becomes unnecessary and G' can be written as follows :

$$G' = \tan^{-1}\frac{f-z}{x-\xi} + 2\,\mathrm{Im}\left[\mathrm{sgn}(x-\xi)\cdot\int_0^\infty \frac{e^{-m|x-\xi|-im(f-z)}}{m+i\kappa_0}\,dm + \pi i\, e^{-\kappa_0(f-z)+i\kappa_0(x-\xi)}\cdot\left\{1+\mathrm{sgn}(x-\xi)\right\}\right] \quad \cdots (15)$$

Furthermore, the integral in the above equation is performed by substituting the real variable m with the following complex variable w, and Y is defined as follows :

$$\left.\begin{aligned} w &= (m + i\kappa_0)\, Y \\ \text{where,}\ \ Y &= |x-\xi| + i\,(f-z) \end{aligned}\right\} \quad \cdots\cdots(16)$$

Accordingly, the integral with m can be rewritten to the following integral with w, and it can be expressed as an exponential integral E_1 for complex arguments [7].

$$\begin{aligned} \int_0^\infty \frac{e^{-m|x-\xi|-im(f-z)}}{m+i\kappa_0}\,dm &= \int_0^\infty \frac{e^{-mY}}{m+i\kappa_0}\,dm = e^{i\kappa_0 Y}\int_0^\infty \frac{e^{-(m+i\kappa_0)Y}}{m+i\kappa_0}\,dm \\ &= e^{i\kappa_0 Y}\int_{i\kappa_0 Y}^\infty \frac{e^{-w}}{w}\,dw = e^{i\kappa_0 Y}E_1\left(i\kappa_0 Y\right) \end{aligned} \quad \cdots\cdots(17)$$

Here, the above equation exhibits the following asymptotic behavior, according to Eq. (45) described in next section, and disappears at infinity $\kappa_0|Y| \to \infty$.

$$e^{i\kappa_0 Y}E_1\left(i\kappa_0 Y\right) \underset{\kappa_0|Y|\to\infty}{\sim} O\left(\frac{1}{\kappa_0|Y|}\right) \quad \cdots\cdots(18)$$

Therefore, the regular part G' in Eq. (15) can be expressed using $E_1\left(i\kappa_0 Y\right)$, as follows :

$$\begin{aligned} G' &= -\tan^{-1}\frac{z-f}{x-\xi} \\ &\quad + 2\,\mathrm{Im}\left[e^{i\kappa_0 Y}E_1\left(i\kappa_0 Y\right)\cdot\mathrm{sgn}(x-\xi) + \pi i\, e^{-\kappa_0(f-z)+i\kappa_0(x-\xi)}\cdot\left\{1+\mathrm{sgn}(x-\xi)\right\}\right] \\ &= -\theta' + 2\,\mathrm{Im}\left[e^{i\kappa_0 Y}E_1\left(i\kappa_0 Y\right)\right]\cdot\mathrm{sgn}(x-\xi) \\ &\quad + 2\pi\, e^{\kappa_0(z-f)}\cos\kappa_0(x-\xi)\cdot\left\{1+\mathrm{sgn}(x-\xi)\right\} \end{aligned} \quad \cdots\cdots(19)$$

Here, the 1st term represents the clockwise vortex $-\theta'$ located at the mirror image position (ξ, f), the 2nd term represents the local disturbance wave due to the property shown in Eq. (18), and the 3rd term represents the trailing free wave generated only downstream $x-\xi>0$.

As a result, the Green's function G in Eq. (9) can be expressed as follows by adding G' in Eq. (19) to the principal solution θ.

$$\begin{aligned} G' &= \left(\tan^{-1}\frac{z+f}{x-\xi} - \tan^{-1}\frac{z-f}{x-\xi}\right) + 2\,\mathrm{Im}\left[e^{i\kappa_0 Y}E_1\left(i\kappa_0 Y\right)\right]\cdot\mathrm{sgn}(x-\xi) \\ &\quad + 2\pi\, e^{\kappa_0(z-f)}\cos\kappa_0(x-\xi)\cdot\left\{1+\mathrm{sgn}(x-\xi)\right\} \\ &\equiv G_r + G_\ell + G_f \end{aligned} \quad \cdots\cdots(20)$$

Here, the sum of the 1st term, the principal solution θ, and the 2nd term, the ordinary mirror image vortex $-\theta'$, is denoted by G_r, and together they satisfy the rigid wall condition at the water surface as shown by Eq. (55) in the section after the next one. The 3rd term corresponds to the local disturbance wave G_ℓ, and the 4th term corresponds to the trailing free wave G_f, as mentioned above.

$E_1(i\kappa_0 Y)$ in the 3rdd term of G_r is the exponential integral extended to complex plane as adopted in Eq. (17), and can be calculated by the following formula :

$$\left.\begin{aligned} E_1(i\kappa_0 Y) &= \int_{i\kappa_0 Y}^{\infty} \frac{e^{-w}}{w}\,dw \\ where,\quad i\kappa_0 Y &= -\kappa_0(f-z) + i\kappa_0|x-\xi| \\ &\equiv -\kappa_0 \hat{f} + i\kappa_0|\hat{x}| \end{aligned}\right\} \quad \cdots\cdots(21)$$

Here, $\hat{f}$ and $\hat{x}$ are abbreviated for the convenience in the following sections, as follows :

$$\left.\begin{aligned} \hat{f} &\equiv f - z \ \ (>0) \\ \hat{x} &\equiv x - \xi \end{aligned}\right\} \quad \cdots\cdots(22)$$

2.3 Calculation method of $E_1(i\kappa_0 Y)$ by switching three expansion forms

The exponential integral $E_1(i\kappa_0 Y)$ of Eq. (21) in the previous section is written by introducing the complex variable η for convenience of analysis, as follows :

$$\left.\begin{aligned} E_1(\eta) &= \int_{\eta}^{\infty} \frac{e^{-w}}{w}\,dw \\ where,\quad \eta &= i\kappa_0 Y = -\kappa_0 \hat{f} + i\kappa_0|\hat{x}| = \kappa_0 R e^{i\Theta} \ \left(for,\ \frac{\pi}{2} < \Theta < \pi \right) \end{aligned}\right\} \quad \cdots\cdots(23)$$

This section explains a method for calculating $E_1(\eta)$ by switching three types of expansion forms, (a) Taylor expansion, (b) continued fraction expansion and (c) asymptotic expansion, depending on the value of η , as the following order :

(a) Taylor expansion

First, let us consider the Taylor expansion [5-b), (8-b)] of $E_1(\eta)$. Since the integrand for $E_1(\eta)$, defined by Eq. (23) on complex plane $w = u + iv$, vanishes at infinity of $u > 0$, $E_1(\eta)$ can be expressed by carefully considering the integration interval such that the path goes through $u = 0$ and $u = 1$ on the real axis, as follows :

$$\begin{aligned} E_1(\eta) &= \left(\int_{\eta}^{1} + \int_{1}^{\infty} \right) \frac{e^{-w}}{w}\,dw = \int_{\eta}^{1} \frac{1-(1-e^{-w})}{w}\,dw + \int_{1}^{\infty} \frac{1-(1-e^{-u})}{u}\,du \\ &= \int_{\eta}^{1} \frac{1}{w}\,dw - \left(\int_{\eta}^{0} \frac{1-e^{-w}}{w}\,du + \int_{0}^{1} \frac{1-e^{-u}}{u}\,du \right) + \left(\int_{1}^{\infty} \frac{1}{u}\,du - \int_{1}^{\infty} \frac{1-e^{-u}}{u}\,du \right) \\ &= -\int_{1}^{\eta} \frac{1}{w}\,dw - \int_{0}^{\eta} \frac{e^{-w}-1}{w}\,dw - \left(\int_{0}^{\infty} \frac{1-e^{-u}}{u}\,du - \int_{1}^{\infty} \frac{1}{u}\,du \right) \\ &= -\log_e \eta - I_2(\eta) - I_{3,4} \end{aligned} \quad \cdots\cdots(24)$$

Here, the 1st term is the logarithmic term, the 2nd term is denoted as I_2, and the 3rd and 4th terms enclosed in parentheses are denoted as $I_{3,4}$.

The exponential function e^{-w} in the integrand of I_2 is expanded into a Taylor series, as follows :

$$e^{-w} = 1 + \sum_{n=1}^{\infty} (-1)^n \frac{w^n}{n!} \quad \cdots\cdots (25)$$

Therefore, by integrating the series term by term, $I_2(\eta)$ is obtained as follows :

$$I_2(\eta) = \sum_{n=1}^{\infty} \left\{ \frac{(-1)^n}{n!} \int_0^{\eta} w^{n-1}\, dw \right\} = \sum_{n=1}^{\infty} \left\{ \frac{(-1)^n}{n!} \left[\frac{w^n}{n} \right]_0^{\eta} \right\} = \sum_{n=1}^{\infty} \left\{ (-1)^n \frac{\eta^n}{n \cdot n!} \right\} \quad \cdots\cdots (26)$$

Regarding $I_{3,4}$, based on the definition of the Napier's constant e, the reciprocal of e can be rewritten by putting $m' = m + 1$, as follows :

$$\frac{1}{e} = \frac{1}{\lim_{m\to\infty} \left(1 + \frac{1}{m}\right)^m} = \lim_{m\to\infty} \left(\frac{m}{m+1} \right)^m = \lim_{m\to\infty} \left(1 - \frac{1}{m+1} \right)^m = \lim_{m'\to\infty} \frac{\left(1 - \frac{1}{m'}\right)^{m'}}{1 - \frac{1}{m'}} = \lim_{m'\to\infty} \left(1 - \frac{1}{m'} \right)^{m'}$$
$$\cdots\cdots (27)$$

Hence, e^{-u} in the integrand of $I_{3,4}$ can be expressed by putting $n = m'u$, as follows :

$$e^{-u} = \left(\frac{1}{e} \right)^u = \left\{ \lim_{m'\to\infty} \left(1 - \frac{1}{m'} \right)^{m'} \right\}^u = \lim_{m'\to\infty} \left(1 - \frac{1}{m'} \right)^{m'u} = \lim_{n\to\infty} \left(1 - \frac{u}{n} \right)^n \quad \cdots\cdots (28)$$

Therefore, substituting the above e^{-u} into $I_{3,4}$ of Eq. (24), it can be calculated by following equation :

$$I_{3,4} = \int_0^{\infty} \frac{1 - \lim_{n\to\infty} \left(1 - \frac{u}{n} \right)^n}{u}\, du - \int_1^{\infty} \frac{1}{u}\, du = \lim_{n\to\infty} \left\{ \int_0^n \frac{1 - \left(1 - \frac{u}{n} \right)^n}{u}\, du - \int_1^n \frac{1}{u}\, du \right\}$$
$$= \lim_{n\to\infty} \left\{ \Psi(n) - \log_e n \right\} \quad \cdots\cdots (29)$$

Here, the 2nd term can be easily integrated and becomes a logarithmic term. $\Psi(n)$ in the 1st term can be obtained by expanding it into a series after performing substitution integration by setting $\tau = 1 - \frac{u}{n}$, and then integrating term by term, as follows :

$$\Psi(n) = \int_0^n \frac{1 - \left(1 - \frac{u}{n} \right)^n}{u}\, du = \int_0^1 \frac{1 - \tau^n}{1 - \tau}\, d\tau$$
$$= \int_0^1 \left(\sum_{j=1}^{n} \tau^{j-1} \right) d\tau = \sum_{j=1}^{n} \left(\int_0^1 \tau^{j-1}\, d\tau \right) = \sum_{j=1}^{n} \left[\frac{\tau^j}{j} \right]_0^1 = \sum_{j=1}^{n} \frac{1}{j} \quad \cdots\cdots (30)$$

Thus, $I_{3,4}$ in Eq. (29) can be obtained as follows, and is found to be Euler's constant γ .

$$I_{3,4} = \lim_{n\to\infty} \left\{ \left(\sum_{j=1}^{n} \frac{1}{j} \right) - \log_e n \right\} = \gamma \ \ (= 0.57721\cdots) \quad \cdots\cdots (32)$$

Therefore, substituting the results from Eqs. (26) and (32) into $I_2(\eta)$ and $I_{3,4}$ in Eq. (24), the exponential integral $E_1(\eta)$ can be expressed as a Taylor expansion form, as follows.:

$$E_1(\eta) = -I_{3,4} - \log_e \eta - I_2(\eta) = -\gamma - \log_e \eta - \sum_{n=1}^{\infty} \frac{(-\eta)^n}{n \cdot n!} \quad \cdots\cdots\cdots\cdots\cdots\cdots\cdots\cdots (33)$$

Now, if we use Euler notation for η, such as $\eta = \kappa_0 R e^{i\Theta}$ from the latter definition of Eq. (23), its absolute value R and argument Θ can be written by using the abbreviations $\hat{f}$ and $\hat{x}$ in Eq. (22), as follows :

$$\left.\begin{aligned} R &= \sqrt{\hat{x}^2 + \hat{f}^2} \\ \Theta &= \tan^{-1}\left(\frac{|\hat{x}|}{-\hat{f}}\right) \end{aligned}\right\} \quad \cdots\cdots\cdots\cdots\cdots\cdots\cdots\cdots\cdots\cdots\cdots\cdots\cdots\cdots\cdots\cdots\cdots\cdots (34)$$

Using the above R and Θ, if we separate $E_1(\eta)$ in Eq. (33) into the real part E_C and the imaginary part E_S, it can be expressed as follows :

$$\begin{aligned} E_1(\eta) &= -\gamma - \log_e \kappa_0 R - \sum_{n=1}^{\infty} \frac{\kappa_0^n R^n}{n \cdot n!} \cdot \cos n(\Theta + \pi) + i \left\{ -\Theta - \sum_{n=1}^{\infty} \frac{\kappa_0^n R^n}{n \cdot n!} \cdot \sin n(\Theta + \pi) \right\} \\ &\equiv E_C + i E_S \end{aligned} \quad \cdots\cdots\cdots\cdots\cdots\cdots\cdots\cdots\cdots\cdots\cdots\cdots\cdots\cdots\cdots\cdots\cdots\cdots (35)$$

For convenience in subsequent calculations, we multiply $E_1(\eta)$ by e^{η} and define its real part by H_C and imaginary part by H_S respectively, as follows :

$$\begin{aligned} e^{\eta} E_1(\eta) &= e^{-\kappa_0 \hat{f} + i\kappa_0 |\hat{x}|} (E_C + i E_S) \\ &= e^{-\kappa_0 \hat{f}} (E_C \cos \kappa_0 |\hat{x}| - E_S \sin \kappa_0 |\hat{x}|) + i\, e^{-\kappa_0 \hat{f}} (E_C \sin \kappa_0 |\hat{x}| + E_S \cos \kappa_0 |\hat{x}|) \\ &\equiv H_C(\eta) + i\, H_S(\eta) \end{aligned} \quad \cdots\cdots\cdots\cdots\cdots\cdots\cdots\cdots\cdots\cdots\cdots\cdots\cdots\cdots\cdots\cdots\cdots\cdots (36)$$

In the above equation, η uses the latter part of Eq. (23).

(b) Continued fraction expansion

Next, according to Abramowitz's Handbook of Mathematical Functions [7], $E_1(\eta)$ in Eq. (23) can be expanded into a continued fraction, as follows :

$$E_1(\eta) = e^{-\eta} \left(\frac{1}{\eta +} \frac{1}{1 +} \frac{1}{\eta +} \frac{2}{1 +} \frac{2}{\eta +} \frac{3}{1 +} \frac{3}{\eta +} \cdots\cdots \frac{n}{1 +} \frac{n}{\eta +} \cdots\cdots \right) \quad \cdots\cdots\cdots\cdots\cdots\cdots\cdots\cdots (37)$$

Specifically, the product of $E_1(\eta)$ and $e^{-\eta}$ above can be expanded in ascending order ($n \to n+1$), as follows :

$$e^{\eta}E_1(\eta)=\frac{1}{\Omega_1}=\cfrac{1}{\eta+\cfrac{1}{1+\cfrac{1}{\Omega_2}}}=\cfrac{1}{\eta+\cfrac{1}{1+\cfrac{1}{\eta+\cfrac{2}{1+\cfrac{2}{\Omega_3}}}}}=\cfrac{1}{\eta+\cfrac{1}{1+\cfrac{1}{\eta+\cfrac{2}{1+\cfrac{2}{\eta+\cfrac{3}{1+\cfrac{3}{\Omega_4}}}}}}} \qquad \cdots\cdots(38)$$

Here, Ω_n in the above is defined by the following equation :

$$\Omega_n=\eta+\cfrac{n}{1+\cfrac{n}{\Omega_{n+1}}}\equiv\varepsilon_n+i\delta_n \qquad \cdots\cdots(39)$$

Since $\eta=-\kappa_0\hat{f}+i\kappa_0|\hat{x}|$ according to the latter of Eq. (23), the real part ε_n and imaginary part δ_n of Ω_n can be continuously calculated in descending order ($n+1\to n$), as follows :

$$\left.\begin{aligned}\varepsilon_n &= -\kappa_0\hat{f}+\frac{n\,(\ell_{n+1}^{\,2}+n\,\varepsilon_{n+1})}{\ell_{n+1}^{\,2}+2n\,\varepsilon_{n+1}+n^2}\\ \delta_n &= \kappa_0|\hat{x}|+\frac{n^2\delta_{n+1}}{\ell_{n+1}^{\,2}+2n\,\varepsilon_{n+1}+n^2}\\ &\textit{whert, } \ell_{n+1}=|\Omega_{n+1}|=\sqrt{\varepsilon_{n+1}^2+\delta_{n+1}^2}\end{aligned}\right\} \qquad \cdots\cdots(40)$$

As for the calculation procedure, starting with the initial term $\Omega_{n+1}=\eta$, we obtain $\varepsilon_{n+1}=-\kappa_0\hat{f}$ and $\delta_{n+1}=\kappa_0|\hat{x}|$. Subsequently, by continuously calculating using Eq. (40), $\Omega_1=\varepsilon_1+i\delta_1$ is determined. After careful consideration, the number of terms to start the calculation was set to n = 15.

As a result, $H_C(\eta)+iH_S(\eta)$ defined in Eq. (36) can be determined using Eq. (40), as follows :

$$\begin{aligned}e^{\eta}E_1(\eta)&=\frac{1}{\Omega_1}=\frac{1}{\varepsilon_1+i\delta_1}=\frac{\varepsilon_1-i\delta_1}{\ell_1^{\,2}}\\ &=H_C(\eta)+i\,H_S(\eta)\end{aligned} \qquad \cdots\cdots(41)$$

(c) Asymptotic expansion

Third, we consider the asymptotic expansion[8-b] of an exponential integral $E_1(\eta)$. By integrating by parts for $E_1(\eta)$ in Eq. (23), it can be written as follows :

$$\begin{aligned}E_1(\eta)&=-\int_\eta^\infty\left(e^{-w}\right)'\cdot\frac{1}{w}\,dw=-\left[e^{-w}\cdot\frac{1}{w}\right]_\eta^\infty+\int_\eta^\infty e^{-w}\left(\frac{1}{w}\right)'dw\\ &=\frac{e^{-\eta}}{\eta}-\int_\eta^\infty\frac{e^{-w}}{w^2}dw\end{aligned} \qquad \cdots\cdots(42)$$

Simulations of Water Wave Generation caused by Running Hydrofoil
by means of Wave-making Green's Function due to 2-D vortex

Performing the same operation 3 times on the integral term, $E_1(\eta)$ can be calculated as follows :

$$E_1(\eta) = e^{-\eta}\left(\frac{0!}{\eta} - \frac{1!}{\eta^2} + \frac{2!}{\eta^3}\right) - 3!\int_\eta^\infty \frac{e^{-w}}{w^4}dw \quad \cdots\cdots(43)$$

Furthermore, by repeating this operation N times, we can obtain the following asymptotic expansion for $E_1(\eta)$:

$$E_1(\eta) = e^{-\eta}\sum_{n=1}^{N}\left\{(-1)^{n-1}\frac{(n-1)!}{\eta^n}\right\} + (-1)^N N!\int_\eta^\infty \frac{e^{-w}}{w^{N+1}}dw \quad \cdots\cdots(44)$$

Here, if the integral term in the 2nd term is omitted as a remainder term when $|\eta| = \kappa_0 R \to \infty$, then real part H_C and imaginary part H_S defined in Eq. (36) can be calculated by using the Euler notation $\eta = \kappa_0 R e^{i\Theta}$ for η , as follows :

$$\begin{aligned} e^{\eta}E_1(\eta) &\underset{|\eta|\to\infty}{\sim} \sum_{n=1}^{N}\left\{(-1)^{n-1}\frac{(n-1)!}{(\kappa_0 R)^n}e^{-in\Theta}\right\} \\ &= \sum_{n=1}^{N}\left\{(-1)^{n-1}\frac{(n-1)!}{\kappa_0^n R^n}\cos n\Theta\right\} - i\sum_{n=1}^{N}\left\{(-1)^{n-1}\frac{(n-1)!}{\kappa_0^n R^n}\sin n\Theta\right\} \\ &= H_C(\eta) + iH_S(\eta) \end{aligned} \quad \cdots\cdots(45)$$

However, since the above equation a divergent series, when the n^{th} term is denoted by a_n and the $(n+1)^{th}$ term by a_{n+1}, the computation of the asymptotic series continues as long as $|a_n| > |a_{n+1}|$ holds.

Based on the above results, the ratio between the two is the former below, so the number of truncated terms N of the asymptotic series is determined by the latter condition below :

$$\left.\begin{aligned} \left|\frac{a_{n+1}}{a_n}\right| &= \frac{n}{|\eta|} = \frac{n}{\kappa_0 R} < 1 \\ &\to N < |\eta| = \kappa_0 R \end{aligned}\right\} \quad \cdots\cdots(46)$$

(d) Calculation method
by switching between (a), (b) and (c)

H_C and H_S were computed radially as shown in Fig. 3, using three types of expansion forms, namely, (a) Taylor expansion in Eq. (36), (b) continued fraction expansion in Eq. (41), and (c) asymptotic expansion in Eq. (45). Specifically, the radial distance $\kappa_0 R = |\eta|$ ranges from 1 to 50, and the argument Θ is indicated in the figure. By comparing the three, we examined which expansion form should be used for which region of 2nd quadrant on the complex plane.

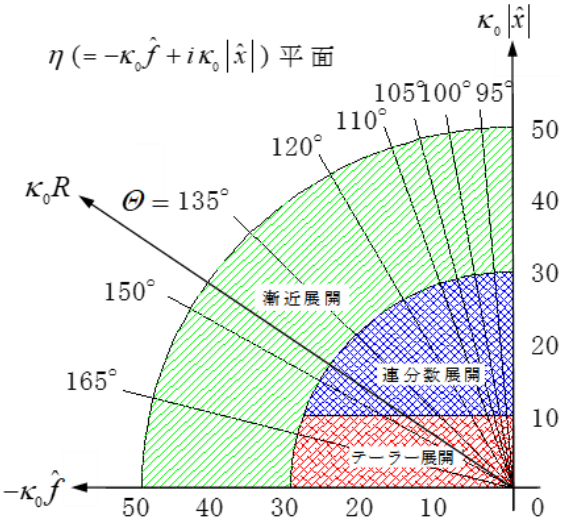

Fig. 3 Domain partitioning in the η -plane.

As a result, in order to switch between the three expansion forms (a), (b) and (c) for calculation, the domain was partitioned as shown in the following equation and Fig. 3 :

$$\left.\begin{array}{l} \kappa_0|\hat{x}|<10,\ \kappa_0 R<30\ :\ (a)\ \textit{Taylor expansion} \\ \kappa_0|\hat{x}|\geq 10,\ \kappa_0 R<30\ :\ (b)\ \textit{Continued fraction expansion} \\ \kappa_0 R\geq 30\ :\ (c)\ \textit{Asymptotic expansion} \end{array}\right\} \quad \cdots\cdots\cdots\cdots\cdots\cdots\cdots\cdots (47)$$

The calculation results, obtained using the above switching method, were confirmed to be correct by comparing them with Abramowitz's Mathematical Tables[7].

2.4 Expression for the derivatives of *G*

We derived the wave-making Green's function G due to a vortex in Section 2.2, but to solve an actual boundary value problem, it is necessary to obtain the expression for the derivatives[8-a] of G with respect to x and z, as shown by the wing surface condition in Eq. (5).

First, let us consider the derivatives of G_ℓ in the 2nd term of Eq. (20). We combine x and z, and denote them collectively by s_j ($j=1, 2$), as follows :

$$s_j=\begin{cases} s_1=x & (j=1) \\ s_2=z & (j=2) \end{cases} \quad \cdots\cdots\cdots\cdots\cdots\cdots\cdots\cdots\cdots\cdots\cdots\cdots\cdots\cdots\cdots\cdots (48)$$

Then, the derivative of the integral exponential $E_1(i\kappa_0 Y)$ in Eq. (21) with respect to Y is calculated by putting $\eta=i\kappa_0 Y$, as follows :

$$\frac{\partial}{\partial Y}E_1(i\kappa_0 Y)=\frac{\partial}{\partial Y}\int_{i\kappa_0 Y}^{\infty}\frac{e^{-w}}{w}\,dw=-\frac{\partial}{\partial \eta}\int_{\infty}^{\eta}\frac{e^{-w}}{w}\,dw\cdot\frac{d\eta}{dY}=-\frac{e^{-\eta}}{\eta}\cdot i\kappa_0=-\frac{e^{-i\kappa_0 Y}}{Y} \quad \cdots\cdots\cdots (49)$$

Therefore, the partial derivative[5-b] of $e^{i\kappa_0 Y}E_1(i\kappa_0 Y)$ with respect to s_j can be obtained[8-b] by using $Y=|\hat{x}|+i\hat{f}$ in Eq. (16) and H_C and H_S in Eq. (36), as follows :

$$\begin{aligned} \frac{\partial}{\partial s_j}\left\{e^{i\kappa_0 Y}E_1(i\kappa_0 Y)\right\} &= \frac{\partial}{\partial Y}\left\{e^{i\kappa_0 Y}E_1(i\kappa_0 Y)\right\}\cdot\frac{\partial Y}{\partial s_j} \\ &= \left\{-\frac{1}{Y}+i\kappa_0 e^{i\kappa_0 Y}E_1(i\kappa_0 Y)\right\}\cdot\frac{\partial Y}{\partial s_j} \\ &= \left[-\left\{\frac{|\hat{x}|}{\hat{x}^2+\hat{f}^2}+\kappa_0 H_S(i\kappa_0 Y)\right\}+i\left\{\frac{\hat{f}}{\hat{x}^2+\hat{f}^2}+\kappa_0 H_C(i\kappa_0 Y)\right\}\right]\cdot\frac{\partial Y}{\partial s_j} \end{aligned} \quad \cdots\cdots\cdots (50)$$

Here, the above $\dfrac{\partial Y}{\partial s_j}$ is obtained from the latter part of Eq. (16), as follows :

$$\left.\begin{array}{l} \dfrac{\partial Y}{\partial s_1}=\dfrac{\partial Y}{\partial x}=\operatorname{sgn}\hat{x} \\ \dfrac{\partial Y}{\partial s_2}=\dfrac{\partial Y}{\partial z}=-i \end{array}\right\} \quad \cdots\cdots\cdots\cdots\cdots\cdots\cdots\cdots\cdots\cdots\cdots\cdots\cdots\cdots\cdots\cdots (51)$$

Then, the derivative of G_ℓ in Eq. (20) with respect to s_j can be calculated as follows :

$$\frac{\partial G_\ell}{\partial s_j} = 2\,\mathrm{Im}\left[\frac{\partial}{\partial s_j}\left\{e^{i\kappa_0 Y}E_1(i\kappa_0 Y)\right\}\right]\cdot \mathrm{sgn}\,\hat{x} \qquad \cdots\cdots(52)$$

Therefore, substituting Eq. (50) and (51) into above, it can be obtained for j=1 and 2, as follows :

$$\left.\begin{aligned}\frac{\partial G_\ell}{\partial x} &= \frac{\partial G_\ell}{\partial s_1} = 2\left\{\frac{\hat{f}}{\hat{x}^2+\hat{f}^2}+\kappa_0 H_C(i\kappa_0 Y)\right\}(\mathrm{sgn}\,\hat{x})^2 = 2\left\{\frac{\hat{f}}{\hat{x}^2+\hat{f}^2}+\kappa_0 H_C(i\kappa_0 Y)\right\}\\ \frac{\partial G_\ell}{\partial z} &= \frac{\partial G_\ell}{\partial s_2} = 2\left\{\frac{|\hat{x}|}{\hat{x}^2+\hat{f}^2}+\kappa_0 H_S(i\kappa_0 Y)\right\}\cdot \mathrm{sgn}\,\hat{x} = 2\left\{\frac{\hat{x}}{\hat{x}^2+\hat{f}^2}+\kappa_0 H_S(i\kappa_0 Y)\,\mathrm{sgn}\,\hat{x}\right\}\end{aligned}\right\} \cdots\cdots(53)$$

Here, in the latter part of the above equation, $|\hat{x}|\mathrm{sgn}\,\hat{x}=\hat{x}$ is used.

Next, the derivatives of G_ℓ in the 1st term of Eq. (20) are easily calculated as follows :

$$\left.\begin{aligned}\frac{\partial G_r}{\partial x} &= -\frac{z+f}{\hat{x}^2+(z+f)^2}+\frac{z-f}{\hat{x}^2+(z-f)^2} = -\frac{2f-\hat{f}}{\hat{x}^2+(2f-\hat{f})^2}-\frac{\hat{f}}{\hat{x}^2+\hat{f}^2}\\ \frac{\partial G_r}{\partial z} &= \frac{\hat{x}}{\hat{x}^2+(z+f)^2}-\frac{\hat{x}}{\hat{x}^2+(z-f)^2} = \frac{\hat{x}}{\hat{x}^2+(2f-\hat{f})^2}-\frac{\hat{x}}{\hat{x}^2+\hat{f}^2}\end{aligned}\right\} \cdots\cdots(54)$$

Here, the above values at $z = 0$ on the still water surface are obtained as below, and the z-component is zero. It can be seen that the ordinary mirror image model satisfies the rigid wall condition.

$$\left.\begin{aligned}\left.\frac{\partial G_r}{\partial x}\right]_{z=0} &= \frac{2f}{\hat{x}^2+f^2}\\ \left.\frac{\partial G_r}{\partial z}\right]_{z=0} &= 0\end{aligned}\right\} \cdots\cdots(55)$$

Then, the derivatives of G_f in the 3rd term of Eq. (20) are also easily calculated as follows :

$$\left.\begin{aligned}\frac{\partial G_f}{\partial x} &= -2\pi\kappa_0(1+\mathrm{sgn}\,\hat{x})\,e^{-\kappa_0\hat{f}}\sin\kappa_0\hat{x}\\ \frac{\partial G_f}{\partial z} &= 2\pi\kappa_0(1+\mathrm{sgn}\,\hat{x})\,e^{-\kappa_0\hat{f}}\cos\kappa_0\hat{x}\end{aligned}\right\} \cdots\cdots(56)$$

Here, by using the abbreviation of Eq. (22) and $z = f - \hat{f}$, Eqs. (54) and (56) above are expressed in terms of $\hat{x}$ and $\hat{f}$.

Based on the above results, the derivatives $\frac{\partial G}{\partial x}$ and $\frac{\partial G}{\partial z}$ of Green's function can be calculated by superposing the three components of G_r in Eq. (54), G_ℓ in Eq. (53) and G_f in Eq. (56) respectively, as follows :

$$\left.\begin{aligned}
\frac{\partial G}{\partial x} &= \frac{\partial G_r}{\partial x} + \frac{\partial G_\ell}{\partial x} + \frac{\partial G_f}{\partial x} \\
&= -\frac{2f-\hat{f}}{\hat{x}^2+(2f-\hat{f})^2} + \frac{\hat{f}}{\hat{x}^2+\hat{f}^2} + 2\kappa_0 H_C(i\kappa_0 Y) - 2\pi\kappa_0(1+\operatorname{sgn}\hat{x})\, e^{-\kappa_0\hat{f}} \sin\kappa_0\hat{x} \\
\frac{\partial G}{\partial z} &= \frac{\partial G_r}{\partial z} + \frac{\partial G_\ell}{\partial z} + \frac{\partial G_f}{\partial x} \\
&= \frac{\hat{x}}{\hat{x}^2+(2f-\hat{f})^2} + \frac{\hat{x}}{\hat{x}^2+\hat{f}^2} + 2\kappa_0 H_S(i\kappa_0 Y)\operatorname{sgn}\hat{x} + 2\pi\kappa_0(1+\operatorname{sgn}\hat{x})\, e^{-\kappa_0\hat{f}} \cos\kappa_0\hat{x}
\end{aligned}\right\} \cdots\cdots\cdots (57)$$

The 2nd term in both equations above is the sum of the 2nd term of Eq. (54), which represents a clockwise ordinary mirror vortex $-\theta'$, and the 1st term of Eq. (53), which represents the local disturbance wave G_ℓ. It can be seen that this represents the induced velocity due to the counterclockwise reverse mirror vortex θ' with the same rotational direction as the principal solution θ placed underwater.

Thus, the sum of the 1st and 2nd terms of Eq. (57) is expressed on the still water surface $\hat{f} = f$, as follows :

$$\left.\begin{aligned}
\left.\frac{\partial G}{\partial x}\right]_{\substack{1st+2nd\ term\ of\ Eq.(57) \\ on\ z=0}} &= -\frac{2f-\hat{f}}{\hat{x}^2+(2f-\hat{f})^2} + \frac{\hat{f}}{\hat{x}^2+\hat{f}^2} = 0 \\
\left.\frac{\partial G}{\partial z}\right]_{\substack{1st+2nd\ term\ of\ Eq.(57) \\ on\ z=0}} &= \frac{\hat{x}}{\hat{x}^2+(2f-\hat{f})^2} + \frac{\hat{x}}{\hat{x}^2+\hat{f}^2} = \frac{2\hat{x}}{\hat{x}^2+f^2}
\end{aligned}\right\} \cdots\cdots\cdots\cdots\cdots\cdots (58)$$

In the case of the reverse mirror image model written above, the *x*-component becomes zero, contrary to the ordinary mirror image one in Eq. (55).

3. Solution Method for Boundary Value Problem and the Lift Force

By solving the boundary value problem, the vortex strength on the wing surface is determined, and the resulting lift force is calculated as the sum of these vortices.

3.1 Method for determining the vortex strength Γ_j

The wing surface condition [*H*] in Eq. (5) can be expressed using the ϕ in Eq. (7), which consists of *n* vortex filaments $\Gamma_j(\xi_j, -f_j)$ and their Green's function $G(x, z\,;\, \xi_j, -f_j)$, as follows :

$$n_x(x,z)\sum_{j=1}^{n}\Gamma_j\frac{\partial G(x,z\,;\,\xi_j,-f_j)}{\partial x} + n_z(x,z)\sum_{j=1}^{n}\Gamma_j\frac{\partial G(x,z\,;\,\xi_j,-f_j)}{\partial z} = 2\pi U n_x(x,z) \quad \cdots\cdots\cdots (59)$$

The above equation must hold at the *n* computational points (x, z), including the trailing edge of the wing, as shown in Fig. 4. Therefore, since it becomes a simultaneous equation with *n* variables in a discrete manner, by solving it, the unknown quantity $\Gamma_j\ (j = 1 \sim n)$ can be determined. Then, the vortex filaments and computational points are densely arranged near the leading and trailing edges of the wing.

In this case, the numerical computations were performed with $n=111$. The Kutta condition [*K*] in Eq. (6) is satisfied by placing the normal vector at the trailing edge on the mean camber line and setting the vortex strength at the trailing edge to $\Gamma_j = 0$.

For a thin wing with a wing thickness of $t=0$, the vortex filaments are placed on an actual camber line with an angle of attack, and the boundary condition [*H*] is satisfied on that line.

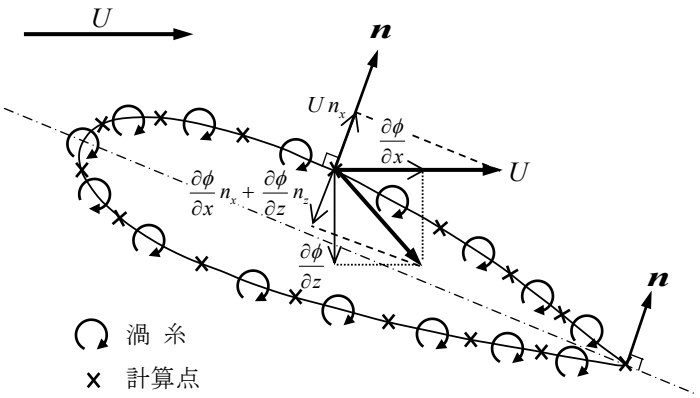

Fig. 4 Arrangement of computational points and vortex filaments on the wing surface.

3.2 Lift Coefficient

Since lift *L* is determined by the summation of the discretely solved vortex strengths Γ_j according to the momentum theorem[6-b], the lift coefficient C_L can be calculated using the following formula :

$$C_L = \frac{L}{\frac{1}{2}\rho U^2 c} = \frac{\rho U \sum_{j=1}^{n} \Gamma_j}{\frac{1}{2}\rho U^2 c} = 2\sum_{j=1}^{n} \frac{\Gamma_j}{Uc} \quad \cdots\cdots\cdots\cdots\cdots\cdots\cdots\cdots\cdots\cdots\cdots\cdots (60)$$

Now, in the following numerical calculation examples, the wing thickness *t*, submerged depth *f,* wave height ζ, and coordinate values *x*, *z* all represent dimensionless lengths based on the wing chord length *c*.

Fig. 5 shows $\frac{C_L}{\alpha}$ for a thin wing of $t=0$ at angles of attack $\alpha = 10°$ and $20°$, which is plotted on *Fn* basis. For shallow submerged depth $f=0.5$, the peak value occurs about $Fn=0.55$. On the other hand, as the depth increases to $f=1.0$ and 3.0, the values approach the theoretical value 2π in an infinite fluid, and the fluctuations caused by *Fn* also become smaller. However, in the case of shallow depth, C_L and α are not in a linear relationship, so the value of $\frac{C_L}{\alpha}$ normalized by α expressed in radians, also takes on different values while the angle of attack a changes, as shown in the figure. Here, *Fn* on the horizontal axis represents the Froude number based on the wing chord length *c*, and as defined

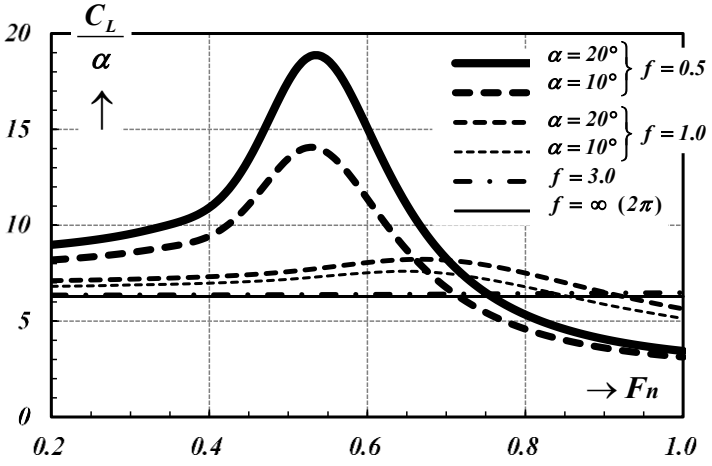

Fig. 5 Lift coefficient of a thin wing
($t=0, \alpha=10°, 20°$)

in the latter part of Eq. (3), it has the following number :

$$Fn = \frac{U}{\sqrt{gc}} = \frac{1}{\sqrt{\kappa_0 c}} \quad \cdots\cdots(61)$$

4. Wave Profile and Wave-Making Resistance

By applying Bernoulli's principle to the water surface $z = \zeta$ and using the fact that no disturbance occurs at infinitely upstream $x \to \infty$, the flow field constants is determined and it can be written as follows :

$$\frac{1}{2}\left\{\left(U + \frac{\partial \phi}{\partial x}\right)^2 + \left(\frac{\partial \phi}{\partial z}\right)^2\right\} + g\zeta = \frac{U^2}{2} \ (= Const.) \quad \cdots\cdots(62)$$

By linearizing the above equation, the wave height ζ can be calculated by the x-component of the disturbed flow velocity on the still water surface $z = 0$. And using the notation of Eq. (8) into $\frac{\partial \phi}{\partial x}$, ζ is obtained in the following form :

$$\zeta(x) = -\frac{U}{g} \cdot \frac{\partial \phi}{\partial x}\Big]_{z=0} = \frac{1}{2\pi\kappa_0 U} \sum_{j=1}^{n} \Gamma_j \frac{\partial G(x, 0\,; \xi_j, -f_j)}{\partial x} \quad \cdots\cdots(63)$$

Furthermore, using the result from Eq. (57) into the above $\frac{\partial G}{\partial x}$, the wave height ζ can be written as follows, and it indicates that ζ is obtained by the superposition of disturbed velocity due to each vortex filament Γ_j. :

$$\zeta(x) = \frac{1}{\pi U} \sum_{j=1}^{n} \Gamma_j \left\{ H_C(-\kappa_0 f_j + i\kappa_0 |x - \xi_j|) - \pi(1 + \mathrm{sgn}(x - \xi_j)) e^{-\kappa_0 f_j} \sin \kappa_0 (x - \xi_j) \right\} \quad \cdots\cdots(64)$$

Here, on $z = 0$, the 1st and 2nd terms of the x-component in Eq. (57) cancel each other out by getting $\hat{f} = f$, as shown in Eq. (58).

Fig 6 shows the wave profiles $\frac{\zeta}{\alpha}$ obtained for the NACA0012 airfoil of $t = 0.12$ with $f = 0.951$, $\alpha = 5°$ and $Fn = 0.567$, and is compared with other results. The vertical axis is the wave height ζ normalized by angle of attack α expressed in radians.

The absolute value of wave height for $t = 0.12$ is larger than that for $t = 0$, and by taking the wing thickness into account, it is approaching Duncan's measured wave profile [9]. Although the absolute value of

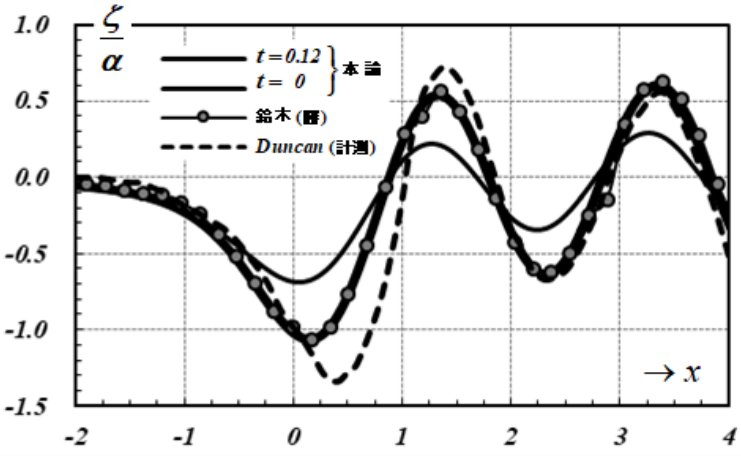

Fig. 6 Comparison of wave profile ζ ($f = 0.951, \alpha = 5°, Fn = 0.567$).

the wave height in the valley directly above at the wing $x \square 0$ is somewhat smaller, it can be seen that they almost overlap downstream. The presented wave profile for $t = 0.12$ overlaps with Suzuki and Hino's calculated value[1] because they were calculated under the same linear free surface conditions.

On the other hand, at infinite downstream $x \to \infty$, the local disturbance H_C of 1st term in Eq. (63) disappears due to the asymptotic characteristics of Eq. (45) and only the trailing free wave of 2nd tem remains, so the wave height ζ can be obtained as follows :

$$\zeta(x) \underset{x\to\infty}{\sim} \frac{2}{U}\left\{\cos\kappa_0 x\sum_{j=1}^{n}\left(\Gamma_j e^{-\kappa_0 f_j}\sin\kappa_0\xi_j\right)-\sin\kappa_0 x\sum_{j=1}^{n}\left(\Gamma_j e^{-\kappa_0 f_j}\cos\kappa_0\xi_j\right)\right\} \quad \cdots\cdots\cdots(65)$$

As a result, the wave amplitude ζ_A at downstream can be calculated by the following equation

$$\zeta_A = \frac{2}{U}\sqrt{\left(\sum_{j=1}^{n}\Gamma_j e^{-\kappa_0 f_j}\sin\kappa_0\xi_j\right)^2+\left(\sum_{j=1}^{n}\Gamma_j e^{-\kappa_0 f_j}\cos\kappa_0\xi_j\right)^2} \quad \cdots\cdots\cdots\cdots\cdots\cdots\cdots\cdots(66)$$

Therefore, the wave-making resistance R_W can be calculated as proportional to the square of the wave amplitude ζ_A in Eq. (66) based on the momentum theorem[5-c], and the wave-making resistance coefficient C_W can be determined as follows :

$$C_W = \frac{R_W}{\frac{1}{2}\rho U^2 c} = \frac{\frac{1}{4}\rho g\zeta_A^{\,2}}{\frac{1}{2}\rho U^2 c} = \frac{1}{2Fn^2}\left(\frac{\zeta_A}{c}\right)^2 \quad \cdots\cdots(67)$$

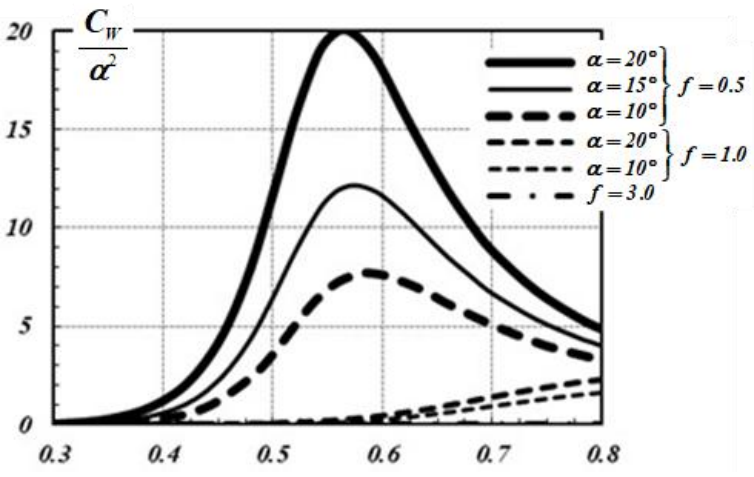

Fig. 7 Wave-making resistance coefficient of thin wing ($t=0, \alpha=10°, 15°, 20°$).

Fig. 7 shows the wave-making resistance coefficient C_W, normalized by α^2, for a thin wing of $t = 0$ similar to Fig. 5, and is plotted against Fn. It can be seen that in the case of shallow submerged depth f, C_W is not proportional to α^2, even when the wing thickness is $t = 0$.

5. Component Separation of Flow Velocity Vectors

Fig. 8 shows the results of a simulation of the flow field around NACA0012 airfoil by separating into its components. The running state of wing is thickness $t = 0.12$, an angle of attack $\alpha = 10°$, the submerged depth $f = 0.5$ and Froude number $Fn = 0.399$. In the figure, the flow velocity vector and wave displacement are drawn superimposed.

Fig. (A) shows the flow in an infinite fluid when the wing is represented by a clockwise underwater vortex, corresponding to the principal solution $-\theta$ of the Green's function in the 1st term of Eq. (57).

Fig. (B) is a flow field generated by a reverse mirror vortex $-\theta'$ located at the aerial mirror image position across the water surface with the same attack angle of underwater wing, corresponding to the 2nd term in Eq. (57). As a result, the flow direction is clockwise, similar to (A).

Fig. (C) shows the velocity component due to the local disturbance wave, corresponding to the 3rd term in Eq. (57). Since the flow generated by this disturbance H_C and H_S is counterclockwise direction, opposite to (B), it represents an ordinary mirror image state placed with an angle of attack opposite to (A). The magnitude of the flow velocity obtained is approximately twice that of (B).

Fig. (D) is the flow field caused by the trailing free wave described by the 4th term in Eq. (57), where there is clearly no flow at upstream of the wing, and the flow velocity becomes nearly zero due to the factor $e^{-\kappa_0 \hat{f}}$ as the water depth increases.

Fig. (E) shows the total disturbed flow velocity superimposed on (A), (B), (C) and (D). Near the downstream water surface, the flow of the trailing free wave from (D) is prominent, while directly above the wing, the flow in the infinite fluid shown in (A) is dominant.

Fig. (F) represents the result of adding a uniform flow to the total disturbed flow drawn in above (E). It can be seen that the flow follows the wing surface around the wing and follows the wave profile near the water surface, so the result demonstrates the validity of this flow simulation.

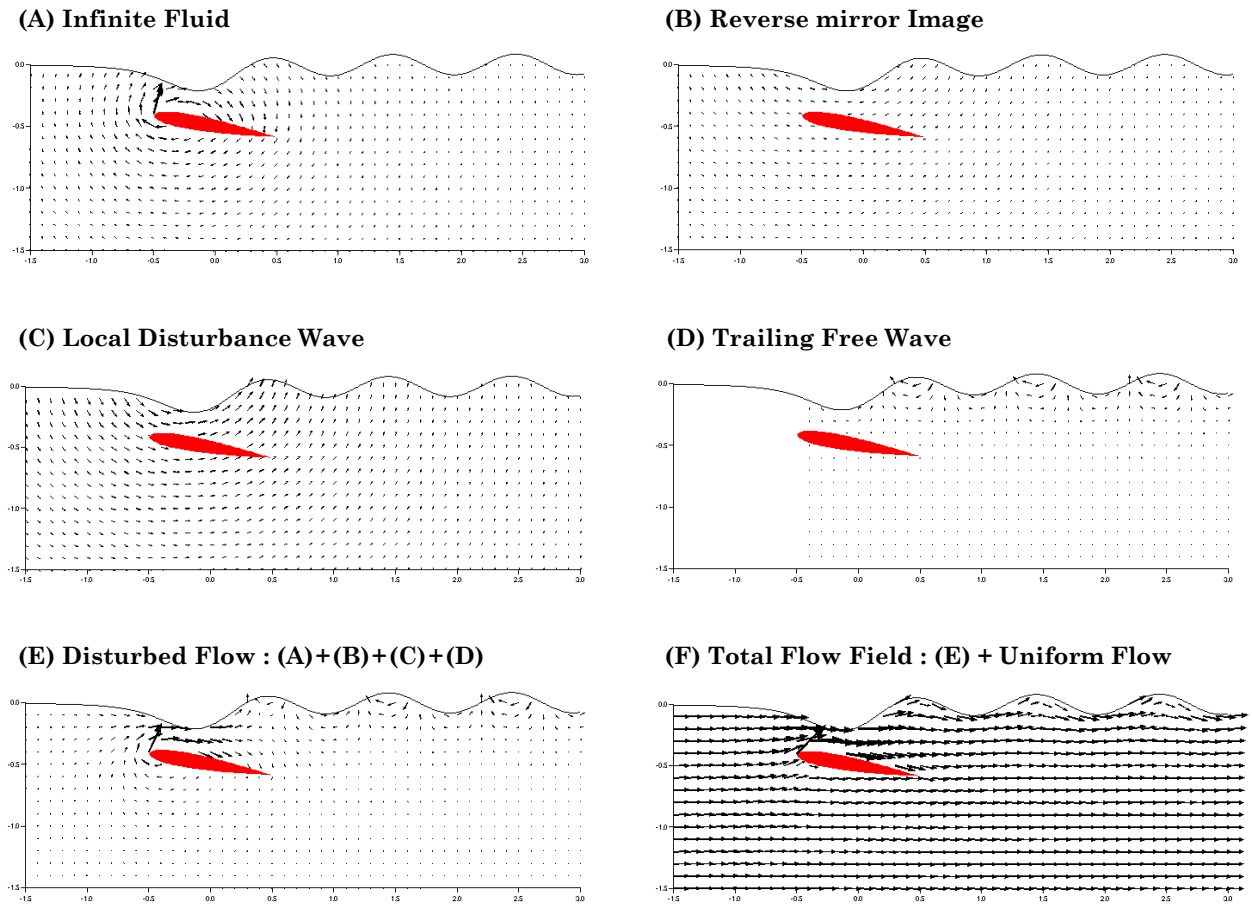

Fig. 8 Components of the flow velocity vector. ($t = 0.12$, $\alpha = 10°$, $f = 0.5$, $Fn = 0.399$).

6. Pressure Distribution

The dynamic pressure around the hydrofoil, excluding hydrostatic pressure $p_0 - \rho g z$ (where p_0 is atmospheric pressure), can be calculated using Bernoulli's principle, as follows :

$$\frac{p-(p_0-\rho g z)}{\rho} = -U\frac{\partial \phi}{\partial x} - \frac{\left(\frac{\partial \phi}{\partial x}\right)^2 + \left(\frac{\partial \phi}{\partial z}\right)^2}{2} \quad \cdots\cdots(68)$$

In deriving the above equation, no disturbance flow occurs at an infinite upstream $x \to \infty$, only uniform flow U remains, so $p = p_0$ was set on the still water surface $z = 0$. And, the disturbance velocities in the above equation can be computed by the superposition of induced velocities from n vortex filaments $\Gamma_j(\xi_j, -f_j)$, as shown in Eq. (8) of Chapter 2.

Fig. 9 shows the pressure distribution around the NACA0012 airfoil of $t = 0.12$ under the calculation conditions of angle of attack $\alpha = 5°$, submerged depth $f = 1.286$ and Froude number $Fn = 0.567$. The results of present method were compared with the numerical solution by Hino [10]. The good agreement between the isobars of both methods confirmed the validity of this calculation method.

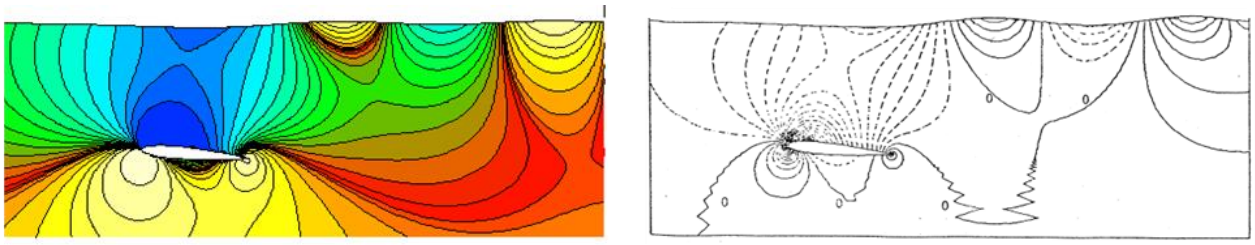

Fig. 9 Comparison of pressure distributions in present method (Left) and Hino (Right).
($t = 0.12$, $\alpha = 5°$, $f = 1.286$, $Fn = 0.567$).

Next, Fig. 10 shows the simulation results for the NACA0024 airfoil with thickness $t = 0.12$, angle of attack $\alpha = 5°$, and submerged depth $f = 0.5$, depicting the changes in isobaric lines, flow velocity vectors, and wave height for advancing speed Fn of 0.55 and 0.77.

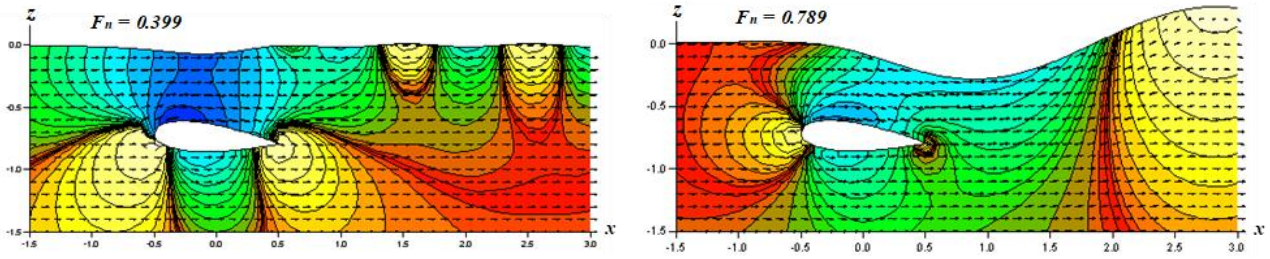

Fig. 10 Isobaric lines, flow vectors, wave profiles for $Fn = 0.399$ (Left) and $Fn = 0.399$ (Right)
($t = 0.24$, $\alpha = 5°$, $f = 0.75$).

7. Simulations of Water Wave Generation

Wave height ζ can be calculated by superimposing the induced velocities in the x-direction on the still water surface from each vortex filament Γ_j, as given by Eq. (67) in Chapter 4.

Fig. 11 simulates the wave generation phenomena for the same NACA0012 airfoil of $t = 0.12$ as in the previous chapter, with fixed submerged depth $f = 0.5$ and angle of attack $\alpha = 5°$, while gradually increasing the Froude number Fn, and is shown by the black thick lines. For comparison, the wave profile approximated as a thin wing of $t = 0$ is shown by the blue thin line. It can be seen that the wave height of generated waves increases depending on the wing thickness.

As shown in the figure, the wavelength of the generated wave increases as the advancing speed Fn increases. Here, the wavelength λ of generated waves, namely the trailing free wave at downstream, is proportional to the square of Fn, in the following form :

$$\frac{\lambda}{c} = \frac{2\pi}{\kappa_0 c} = 2\pi Fn^2 \quad \cdots\cdots (69)$$

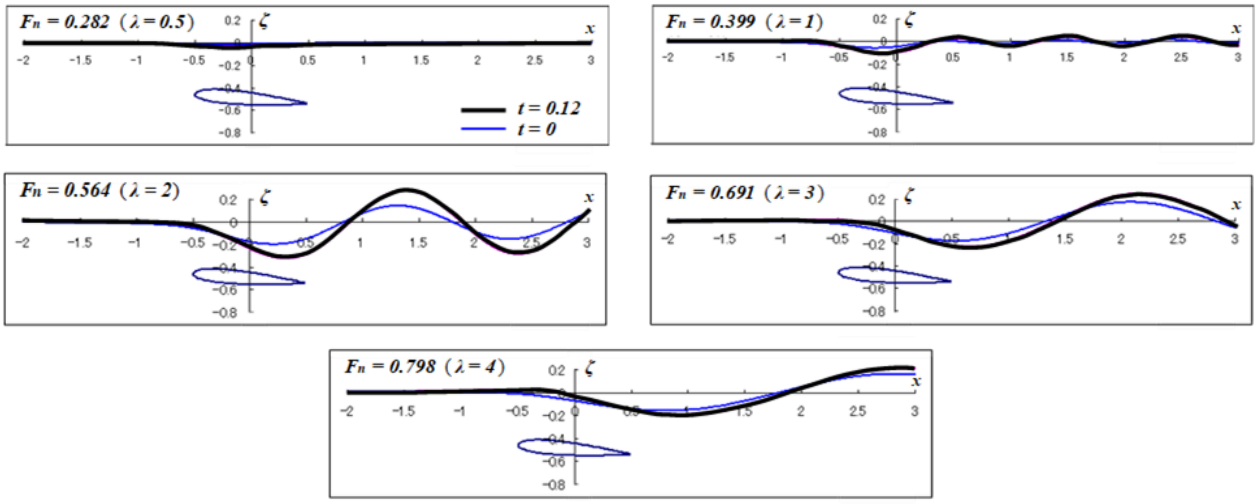

Fig. 11 Simulation of varying Froude number Fn ($f = 0.5$, $\alpha = 5°$).

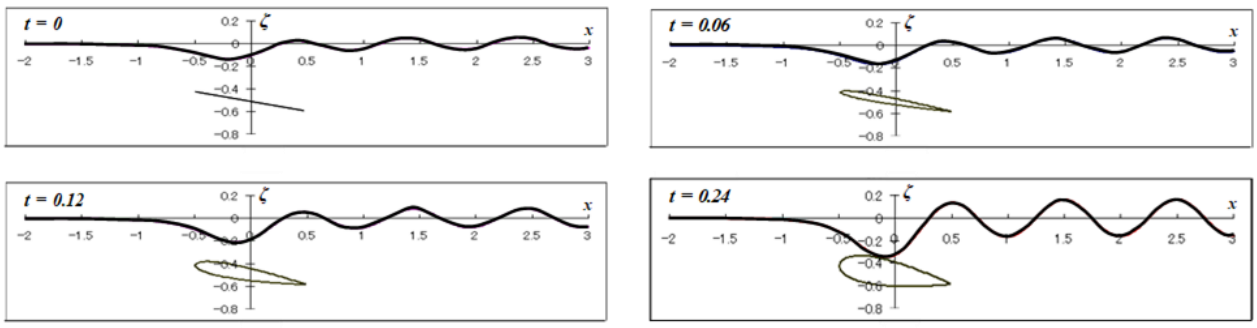

Fig. 12 Simulation of varying thickness t ($\alpha = 10°$, $f = 0.5$, $\alpha = 5°$, $Fn = 0.399$).

Next, Fig. 12 is simulations of the generated waves for the angle of attack $\alpha = 10°$, submerged depth $f = 0.5$ and Froude number $Fn = 0.399$ fixed all, while varying the thickness t of the NACA airfoil. It can be seen that increasing the wing thickness also increases the wave height, as similar to Fig.11.

Furthermore, Fig. 13 shows the result of simulations for the fixed submerged depth $f = 0.6$, Froude number $Fn = 0.399$ and thickness $t = 0.12$, while varying the angle of attack α. Similar to Fig. 11, it also shows the wave profile approximated as thin wing $t = 0$, depicted by blue lines. This indicates that the increase in wave height with increasing angle of attack is well simulated.

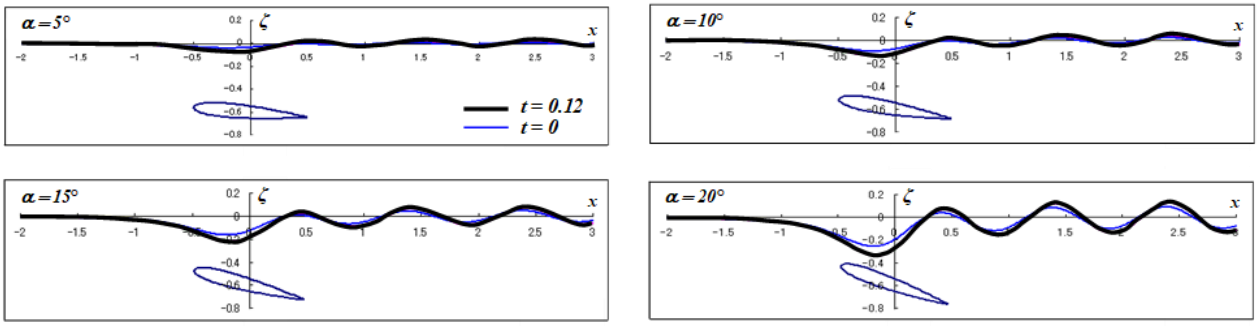

Fig. 13 Simulation of varying angle of attack α ($f = 0.6$, $Fn = 0.399$).

8. Concluding Remarks

Wave-making simulations of a hydrofoil running at high speed were performed for NACA wings using a boundary element method based on wave-making Green's function due to a two-dimensional vortex filaments, developed by authors. In the numerical calculation of the Green's function, we proposed a computational method that switches between three types of expansion forms, namely, Taylor expansion, continued fraction expansion, and asymptotic expansion, depending on the case.

It was confirmed that the lift and wave-making resistance acting on a hydrofoil can be computed with high precision, and that the flow field and pressure distribution around the hydrofoil and the generated waves can be accurately simulated. As a result, quantitative insights were obtained regarding the dependence of the wave-making phenomena on wing thickness, Froude number, submerged depth, angle of attack and other factors.

The future challenge is extending this approach to three-dimensional problems.

Acknowledgments

In closing this paper, we would like to express our deepest gratitude to Manabu KANATA, Koji SUZUKI, and Hiroyuki UEDA, who performed diligently with us on the numerical calculations for this study as part of their graduation research project in the Department of Naval Architecture at Nagasaki Institute of Applied Science, Japan.

In addition, it should be noted that flow velocity vectors and isobaric lines in Chapters 5 and 6 are drawn by using Gsharp of Ver. 2.0 for Windows, a graphing software developed by Japan Electronics Computer Co., Ltd..

References ‡

(1) Suzuki, K. and Hino, T. : " Calculation of Waves generated by a Submerged Hydrofoil " (in Japanese), *Text of the Computational Ship Fluid Dynamics Forum*, Research Group of the Computational Ship Fluid Dynamics, 1987 (December), pp.107~128.

(2) Shin, M. and Mori, K. : "Numerical Computation of 2-Dimensional Waves behind a Hydrofoil", *Journal of the Society of Naval Architects of Japan,* 1988 (June), ***Vol.163***, pp.17~22.

(3) Nakatake, K., Kawagoe, T., Kataoka, K. and Ando. J. : "Calculation of the Hydrodynamic Forces Acting on a Hydrofoil " (in Japanese), *Transactions of the West-Japan Society of Naval Architects*, 1988 (August), ***No.76***, pp.1~13.

(4) Hori, T. : " Simulation Study of Water Wave Generation Caused by Running 2-D Hydrofoil " (in Japanese), ***NAVIGATION*** (*Transactions of Japan Institute of Navigation*), 2016 (April), ***No.196***, pp.99~108.

(5) Hori, T. : "Seminar on Ship Hydrodynamics" (in Japanese), ***Chapter 2*** : Water Waves generated by a Circular Cylinder, ***Chapter 3*** : Wave-making Resistance acting on a Circular Cylinder, ***Lecture Note*** *of Nagasaki Institute of Applied Science Graduate School Master's Program*, 1997 (September).
(a) Section 2.5 : Flow Field around a Submerged Circular Cylinder
placed under the Free Surface, pp.24~28.
(b) Appendix F : Exponential Integral Function Ei extended to the complex plane, pp.28~30.
(c) Section 3.1 : Formula of Wave-making Resistance based on Momentum Theorem, pp.33~36.

(6) Hori, T. and Hori, M. : "Analysis on Aerodynamic Characteristics of WIG －Proposal of New Green's Function Considering Water Wave Generation Caused by Aerial Vortices －", 2025 (September), ***viXra.org*** *(Pre-print Repository, Scientific GOD Inc.),* ***viXra:2509.0066*** [Ver.1], Classical Physics.
(a) Chapter 3 : Expression of Wave Height ζ , pp.7~11.
(b) Section 5.1 : Lift Force, pp.15~16.

(7) Abramowitz, M. and Stegun, I. A. (Editor) : " Handbook of Mathematical Functions With Formulas, Graphs, and Mathematical Tables ", Chapter 5 : Exponential Integral and Related Functions (Author : Gautschi, W. and Cahill, W. F.), Applied Mathematics Series 55, National Bureau of Standards, U.S. Department of Commerce, 1964 (June), p.227~251.

(8) Hori, T. : "A Numerical Analysis of the Neumann-Kelvin Problem on Steady Wave Generation －(1st Report) Some Numerical Discussions for a Two-Dimensional Submerged Circular Cylinder－" (in Japanese), *Bulletin of Nagasaki Institute of Applied Science*, 1992 (October), ***No.33*** (50th Anniversary Commemorative Issue).
(a) Section 2.3.2 : Expression for the Derivative of G, and,
Section 2.3.3 : Calculation Example of Green's Function and Its Derivative, pp.166~169.
(b) Appendix A : Calculation Method of Exponential Integral Function Ei, pp.182~184.

(9) Duncan, J. H. : " The Breaking and Non-Breaking Wave Resistance of a Two-Dimensional Hydrofoil ", *Journal of Fluid Mechanics*, *Vol.126*, 1983 (January), pp.507~520.

(10) Hino, T. : " Numerical Computation of a Free Surface Flow around a Submerged Hydrofoil by the Euler / Navier-Stokes Equations ", *Journal of the Society of Naval Architects of Japan,* 1988 (December), ***Vol.164***, pp.9~17.

‡ Bold text in the list means that there is a HyperLink.

Theoretical Hydrostatics of Floating Bodies

— New Developments on the Center of Buoyancy, the Metacentric Radius and the Hydrostatic Stability —

Written by Tsutomu HORI
Edited by Manami HORI

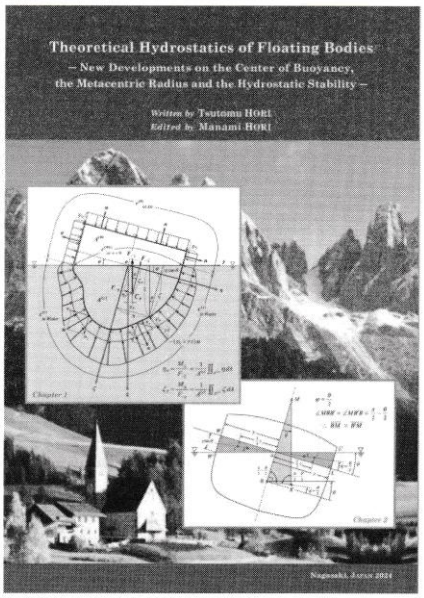

A4判，108ページ，ハードカバー，¥2,200（税込み）
発行：2024年9月，ISBN 978-4-86741-253-4，販路：Amazon

■内容紹介

浮体静力学の基礎理論に関する新展開として，「浮心＝圧力中心」の証明（第1章），メタセンター半径導出の新理論（第2章）と，その復原性への応用（第3，4章）について，最新の研究成果を，解り易く説明しています。

説明は英文ですが，数式の展開を懇切に書いていますし，理論を説明する図も詳細に描いています。読み進むことによって，理論の醍醐味を味わって頂くことが，著者（堀　勉；長崎総合科学大学・名誉教授）と 編者（堀　愛美）の願いです。

航海学や造船学を学ぶ学部生や大学院生の皆さんは，本書を読んだ上で，応用的な専門科目を学んで頂くと，大いなる展望が拓けると思います。

☞ https://www.v2-solution.com/booklist/978-4-86741-253-4.html

(株)ブイツーソリューション発行 〒466-0848 愛知県名古屋市昭和区長戸町4-40 TEL 052-799-7391 FAX 052-799-7984